RESEARCH ARTICLE

Long term bed rest with and without vibration exercise countermeasures: Effects on human muscle protein dysregulation

Manuela Moriggi[1], Michele Vasso[1,2], Chiara Fania[1], Daniele Capitanio[1], Gaetano Bonifacio[1,2], Michele Salanova[3], Dieter Blottner[3], Jörn Rittweger[4], Dieter Felsenberg[5], Paolo Cerretelli[6] and Cecilia Gelfi[1,6]

[1] Dipartimento di Scienze e Tecnologie Biomediche, Università degli Studi di Milano, Milano, Italy
[2] LATO HSR Giglio, Palermo, Italy
[3] Charité-Universitätsmedizin Berlin, Campus Benjamin Franklin, Vegetative Anatomy and Zentrum für Weltraummedizin Berlin, Berlin, Germany
[4] Institute for Biophysical and Clinical Research into Human Movement, Manchester Metropolitan University, Manchester, England
[5] Charité-Universitätsmedizin Berlin, Campus Benjamin Franklin, Zentrum fur Muskel und Knochenforschung, Berlin, Germany
[6] Istituto di Bioimmagini e Fisiologia Molecolare, CNR, Milano, Italy

The present investigation, the first in the field, was aimed at analyzing differentially, on individual samples, the effects of 55 days of horizontal bed rest, a model for microgravity, on myosin heavy and myosin light chain isoforms distribution (by SDS) and on the proteome (by 2-D DIGE and MS) in the *vastus lateralis* (VL), a mixed type II/I (~50:50%) head of the quadriceps and in the calf *soleus* (SOL), a predominantly slow (~35:65%) twitch muscle. Two separate studies were performed on six subjects without (BR) and six with resistive vibration exercise (RVE) countermeasures, respectively. Both VL and SOL underwent in BR decrements of ~15% in cross-sectional area and of ~22% in maximal torque that were prevented by RVE. Myosin heavy chain distribution showed increased type I and decreased type IIA in BR both in VL and in SOL, the opposite with RVE. A substantial downregulation of proteins involved in aerobic metabolism characterized both in SOL and VL in BR. RVE reversed the pattern more in VL than in SOL, whereas proteins involved in anaerobic glycolysis were upregulated. Proteins from the Z-disk region and from costamers were differently dysregulated during bed rest (both BR and RVE), particularly in VL.

Received: December 11, 2009
Revised: July 6, 2010
Accepted: August 3, 2010

Keywords:
2-D DIGE / Bed rest / Biomedicine / Exercise countermeasures / Mass Spectrometry / Muscle

Correspondence: Professor Cecilia Gelfi, Dipartimento di Science e Tecnologie Biomediche, Università degli Studi di Milano, L.I.T.A., Via Fratelli Cervi 93, 20090 Segrate (Milano), Italy
E-mail: cecilia.gelfi@unimi.it
Fax: +39-0250330414

Abbreviations: AHR, aryl hydrocarbon receptor; **BR,** bed rest without countermeasures; **BVA,** biological variation analysis; **CSA,** cross-sectional area; **DIA,** differential in-gel analysis; **IPA,** Ingenuity Pathway Analysis; **MyHC,** myosin heavy chains; **MyLC,** myosin light chains; **PGC-1α,** peroxisome proliferator-activated receptor γ coactivator-1α; P_o, peak force; **RVE,** bed rest with resistive vibration exercise; **SOL,** *soleus*; **VL,** *vastus lateralis*; V_o, peak shortening velocity

1 Introduction

Bed rest, with or without a 6° head down tilt, is an appropriate model for eliminating the weight-bearing function in man and a widely accepted space flight analog procedure for human research whereby the pull of gravity is not suppressed but shifted by 90° [1]. It has been adopted for the studies of respiratory, cardiovascular, bone and, particularly, muscle adaptive changes. With regard to the latter tissue, bed rest is known to induce substantial atrophy in lower limb muscles characterized by reduced cross-sectional area (CSA) and fascicle length. Muscle mass

decreases according to an approximately exponential function of time. This conclusion applies to several back and limb muscles comprising the *vastus lateralis* (VL), a head of the quadriceps, a mixed fast or type II/slow or type I (~50:50%) and the calf *soleus* (SOL), a predominantly slow (~35:65%) twitch muscle. The decrease in muscle mass appears to attain an asymptote after 6–9 months at ~70% of the control level [2–8]. Muscle atrophy is accompanied by a loss of maximum torque, the decrease of which is greater than that in muscle CSA [9–11], likely a consequence of decreased myofibrillar density [12–13]. The same trend applies to the development of maximum instantaneous (''peak'') power by lower limbs [14]. With regard to fiber size and mechanical properties, peak force (P_o) and peak shortening velocity (V_o) were found to vary in chemically skinned type I SOL fibers as a function of bed rest duration [3, 6, 10, 15]. There appears to be agreement on a fiber diameter decrement, decreased P_o *per* CSA unit, and increased or constant V_o, compensating for peak power development. With regard to contractile proteins, after 37 days of bed rest, myosin heavy chain (MyHC) bands were characterized by 38% weaker staining on SDS-PAGE, indicating that the muscle fibers myosin content decreases in response to unloading. In addition, electrophoretic protein analysis of single fiber segments of the quadriceps muscle indicates that MyHC, C-protein and actin, decreases in the same proportion in response to 37 days of bed rest with only a change in the isoform distribution of the regulatory myosin light chains (MyLC) [10].

As is well known, the loss of muscle mass during BR is brought about by a perturbed anabolic (synthesis)-catabolic (breakdown) protein balance leading to a loss of muscle nitrogen. The primary adaptive response appears to be a decrease in protein synthesis [16–19] without any increased breakdown of myofibrillar proteins by proteolytic enzymes and/or by activation of the ubiquitin–proteasome pathway [20–23]. Recent study has shed light also on circuits controlling skeletal muscle hypertrophy such as IGF-1/PI3K/AKT/mTOR signalling pathway known to promote protein synthesis and on the control of protein degradation and expression of ''atrogens'' [24, 25]. This was the case also for the role of the transcriptional coactivator, peroxisome proliferator-activated receptor γ coactivator-1α (PGC-1α), a master regulator of mitochondrial biogenesis and atrogens program that is induced in response to exercise [26–28].

The recent progress in muscle proteomics [29–33], particularly the development of differential analysis, allows to study structural, contractile, metabolic, stress response and transport proteins modulation thereby providing a powerful tool also for the study of functional adaptation of muscle to bed rest. Thus, in view of future comparative studies on the astronaut, it appeared of paramount importance to analyze the protein signature of lower limbs muscle adaptation during bed rest without and with exercise countermeasures [7, 34].

The aims of the present investigation are as follows:

(i) To analyze differentially, individually and in triplicate, the muscle proteome of the VL and of the SOL muscle before and after 55 days of horizontal bed rest without (BR) and with resistive vibration exercise (RVE) countermeasures. Preliminary structural and ultrastructural data of muscle mass and maximum torque as well as of fiber type distribution for the investigated subjects were obtained from the experimental protocol of a previous study by some of the authors [35].

(ii) To quantitatively assess in individual samples the levels of transcriptional coactivator PGC-1α known to increase mitochondrial biogenesis in response to training and to promote fiber-type switching from glycolytic toward more oxidative fibers, in the two investigated muscles and the relationship of its expression with proteome changes.

(iii) To identify possible associations of the observed protein changes with some biological key networks by Ingenuity Pathway Analysis (IPA).

2 Materials and methods

2.1 Subjects

In total, 12 subjects participating in the 55-day bed rest study organized during the period 2003–2004 by the European Space Agency (ESA) and the Centre of Space Medicine Berlin at the Charitè University Medicine Berlin, Berlin (Germany) were selected for this study. The candidates were randomly assigned to two groups of six subjects, the BR one and the one undergoing bed rest with countermeasures (RVE) (Table 1). The caloric intake of the subjects was controlled in order to maintain the body mass relatively constant. Nutritional supervision was assured on recommendation of the German Society of Nutrition. All subjects gave their informed consent and the study was approved by the ethical committee of the collaborating institutions.

Table 1. Physical and physiological characteristics of the investigated subjects (mean $\pm$ SD)

Subjects	BR (six)	RVE (six)
Age (years)	32.7 $\pm$ 7.2	33.2 $\pm$ 6.1
Height (cm)	182 $\pm$ 6.5	187.2 $\pm$ 7.2
Weight (kg)	75.6 $\pm$ 5.5	82 $\pm$ 10.5
VO_2max (mL kg^{-1} min^{-1})	42.4 $\pm$ 6.7	37.1 $\pm$ 10
BMI	22.6 $\pm$ 2.8	24.1 $\pm$ 2.3

2.2 Muscle mass, structural and physiological measurements

Left quadriceps mass and CSA were determined by Magnetic Resonance Imaging. The mass of the right calf muscle was obtained by Computed Tomography. Muscle samples were taken on the second day of bed rest and close to the end of the bed rest period (55th day) from the VL of the left hip flexor/knee extensor quadriceps muscle, and from the right calf SOL muscle (plantar flexor) according to the method of Bergstrom [36]. Attempts were made to extract the samples at approximately the same location in all individuals.

2.3 Exercise measurements

Knee extensor and plantar flexor maximum torque levels were determined on a force platform. RVE was carried out by means of a vibrating foot platform (Galileo Space, Novotec, Pforzheim, Germany) feasible for a frequently repeated training protocol throughout prolonged bed rest immobilization. The subjects, in supine position, were attached to the device by elastic belts with hips, shoulders and hands [37], and the resting static force (Frest), depending on the two selected protocols (morning or afternoon daily session), varied between 200 and 140% of the subjects' body weight. Vibrations (19–25 Hz) were generated by means of eccentrical anti-phase rotation of two masses under the feet on the opposite side of the foot platform. Hence, each side of the platform accelerates alternatively the left leg toward the head of the subject, whereas the right leg is extending. The amplitude of the vibration being preset, the acceleration increases with the vibration frequency and so does the resistive-like force exerted by the extensor and flexor muscles. The amplitude of the vibration results from the acceleration of the platform and the resistive force of the leg extension and was usually in the range of 0.5–1 cm. The applied protocol consisted of two daily bouts (6 min each) at preset frequencies ranging from 19 at the beginning to 25 Hz toward the end of the bed rest period for a total of 89 sessions. Four different exercise units were performed in each session (squats, involving knee extensors; heel raises, activating foot plantar flexors; toe raises, activating foot dorsi-flexors and kiks, whereby knees were extended as quickly and forcefully as possible). During each session, the above-mentioned exercise units were carried out in ascending order. Thus, training intensity was controlled by the resting force (Frest), vibration frequency which increased throughout the bed rest period and the duration of each exercise unit.

2.4 Muscle differential proteome profile

Muscle biopsies from VL and SOL from 12 healthy subjects (males, age range 24–43 years) involved in the "Berlin Bed Rest Study-1" (BBR-1) before and after 55 days of bed rest, six without (BR) and six with countermeasures (RVE), were analyzed by a quantitative 2-D DIGE protocol. The two sets of samples were processed separately and at different times as imposed by the availability of the material based on the experimental protocol [35]. This implied the use of two separate internal standards. 2-D DIGE methods and results were obtained and inserted in an MIAPE-GE compliant form [38] in Supporting Information Table 1S.

2.4.1 Protein extraction

Frozen muscles of each individual were ground in a frozen mortar, suspended in sample buffer (7 M urea, 2 M thiourea, 4% CHAPS, 30 mM Tris, 1 mM PMSF) and solubilized by sonication on ice. Proteins were selectively precipitated using PlusOne 2D-Clean up kit (GE Healthcare) in order to remove non-protein impurities, and re-suspended in lysis buffer. The pH of the protein extracts was adjusted to 8.5 by addition of 1 M NaOH. Protein concentrations were determined by PlusOne 2D-Quant Kit (GE Healthcare).

2.4.2 CyDye labelling and experimental design

Protein minimal labelling with cyanine dyes (Cy3 and Cy5) was performed, according to the manufacturer's recommendations, by mixing 50 μg of individual sample extracts with 400 pmol CyDye (CyDye DIGE Fluor minimal dye, GE Healthcare) and incubating on ice in the dark for 30 min. The labelling reaction was quenched with 1 μL L-lysine 10 mM on ice for 10 min in the dark. Proteins extracted from each individual muscle (VL and SOL) were labelled with Cy5. Internal standards were generated by pooling individual samples before and after bed rest from VL and SOL (BR and RVE) and were Cy3 labelled. The inclusion of an internal standard improves the matching of intra- and inter-gel images and allows normalization across all gels [39]. The experimental design is shown in Fig. 1. The "two dyes" protocol was adopted. Since a double laser beam scanner was available, the analysis was performed utilizing the combination of Cy3/Cy5, due to their labelling efficiency and reliability compared with other dye combinations as described previously [40–42]. No preferential protein labelling or background noise were observed, and thus a larger gel number was required compared with the three dyes protocol. By utilizing the two dyes combination and the manufacturer's dye/protein ratio, no dye swap was needed since all samples undergoing the statistical analysis were labelled with the same dye (Cy5) and were normalized against the same internal standard (Cy3 labelled).

2.4.3 2-D DIGE

Before isoelectric focusing, labelled samples were diluted in an equal volume of 2 × sample buffer containing 130 mM

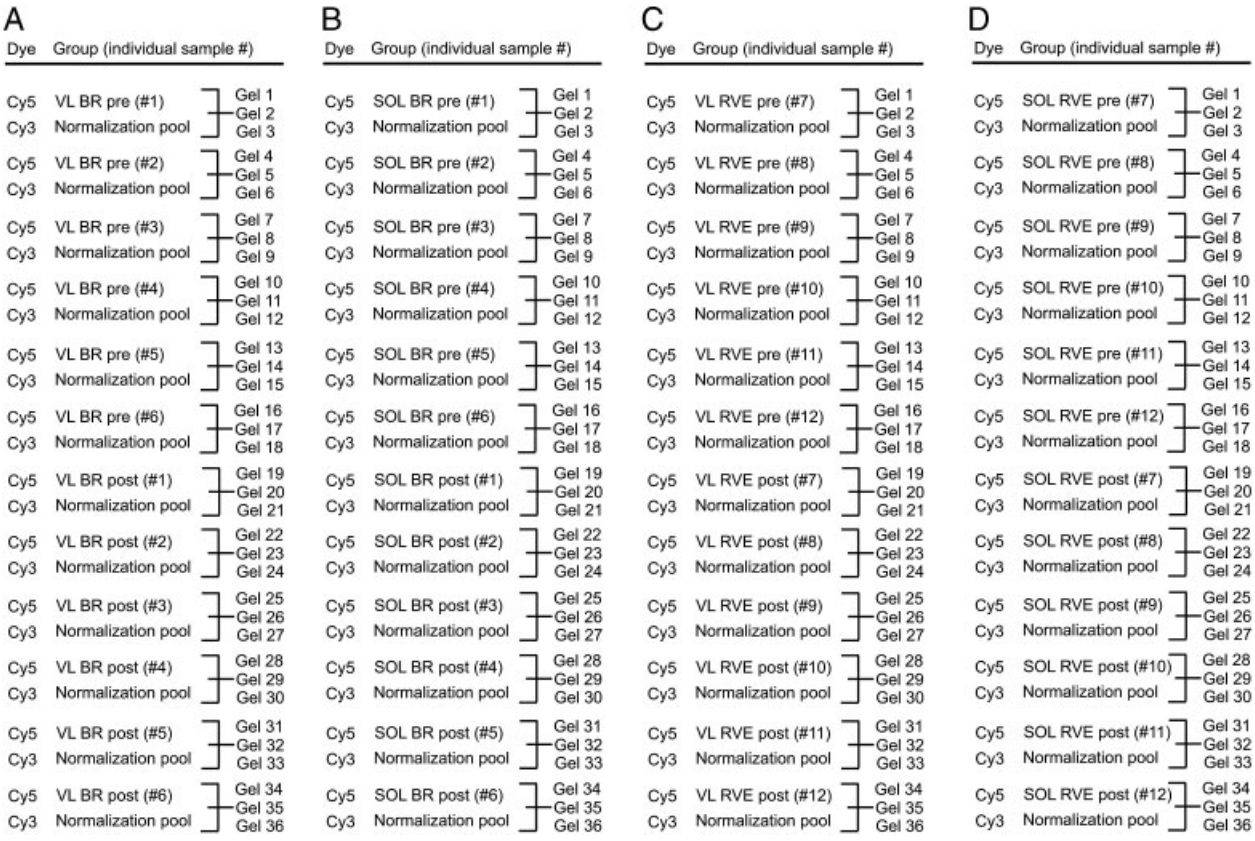

Figure 1. 2-D DIGE experimental design. Protein extracts from VL and SOL of 12 healthy subjects (males, age range 24–43 years) enrolled in the ''Berlin Bed Rest Study-1'' before and after 55 days of bed rest, six BR and six with RVE countermeasures were analyzed using a quantitative 2-D DIGE protocol. Proteins extracted from each individual sample were labelled with Cy5. Internal standards were generated by combining 50 μg of protein from each individual samples (BR and RVE) of VL and SOL and labelled with Cy3. The internal standard was co-separated with the sample to normalize quantitation across gels. Four different analyses were performed: (A) VL post- *versus* pre-BR; (B) SOL post- *versus* pre-BR; (C) VL post- *versus* pre-RVE; (D) SOL post- *versus* pre-RVE.

DTT and 2% v/v IPG buffer (GE Healthcare). Samples from each individual (40 μg) were combined with an equal amount of internal standard, total protein loaded on the gel was 80 μg; rehydration buffer (7 M urea, 2 M thiourea, 2% CHAPS, 65 mM DTT, 0.5% IPG buffer pH 3.5–9.5 and BBF in traces) was added to a final volume of 450 μL. Samples were separated on 24 cm, 3–10 nonlinear pH gradient IPG strips, with a voltage gradient ranging from 200 to 8000 V, for a total of 70 000 VhT, using an IPGphor electrophoresis unit (GE Healthcare). Each individual sample was run in triplicate to minimize the inter-gel variability and to increase the reliability of the results. After focusing, IPG strips were equilibrated in an SDS-reducing buffer (6 M urea, 2% SDS, 20% glycerol, 375 mM Tris-HCl pH 8,8, 65 mM DTT) for 15 min, then alkylated for 8 min in the same buffer containing 135 mM iodoacetamide instead of DTT. The second dimension was carried out in $20 \times 25\ cm^2$, 12% T, 2.5% C constant concentration polyacrylamide gels at 20°C and 15 mA *per* gel using the Ettan Dalt II system (GE Healthcare).

2.4.4 Image acquisition and gel analysis

CyDye-labelled gels were visualized and acquired using a Typhoon 9200 Imager (GE Healthcare). Excitation and emission wave lengths were chosen according to the manufacturer's recommendations (Cy3, Ex = 532 nm, Em = 580 nm BP 30; Cy5, Ex = 633 nm, Em = 670 nm BP 30). Resolution was of 100 μm and the photomultiplier voltage set to a level where the most abundant spots were slightly beneath saturation. Image analysis was performed using the DeCyder version 6.5 software (GE Healthcare). All gel images were imported into individual DIA (differential in-gel analysis) workspaces. Using the Batch Processor tool, automated detection of protein spots was performed with the following filter settings: estimated number of spots = 10 000, exclusion slope >1.2, minimal area cut-off <200 and peak height <14>100 000. DIA workspaces were then manually edited to eliminate gel artefacts (*e.g.* plate scratches and dust specks) and to re-include any incorrectly excluded spot. The resulting spot maps (containing the spot identifiers, locations and normalized volumes for all protein

spots in each channel of each gel) were further processed in the biological variation analysis (BVA) module. Individual DIA workspaces for all analytical gels were imported into the BVA module. The BVA workspace was used for inter-gel protein spot matching. Detailed DIA and BVA information are summarized in Supporting Information Table 2S. Statistical analysis was performed using DeCyder EDA module version 1.0 (Extended Data Analysis). Protein filters were set to select only those protein spots that matched at least on 90% of the gel images, and these protein spots were included in data analysis. The paired Student's *t*-test ($p < 0.05$) was used to determine the protein spots that were significantly different between analyses. The paired test can be used because each data point in a group corresponds to a matching data point in a other group. To minimize inclusion of false-positive protein spot changes, protein expression data were filtered by the following criteria: paired Student's *t*-test ($p < 0.05$), 1.15-fold difference in abundance and false discovery rate. The change of 1.15-fold and above in protein abundance was considered for the present analysis, taking into account the power of the DIGE method to detect reliable difference in protein abundance down to 15% [43, 44]. False discovery rate correction was applied as multiple testing correction method to keep the overall error rate as low as possible [45]. Proteins of interest were identified by MALDI-ToF MS/MS or HPLC ESI MS/MS. Differential results were validated for a selected number of proteins by Western blotting (Supporting Information Figs. 1S and 2S) on the samples previously analyzed by 2-D DIGE.

2.4.5 Protein identification by MALDI ToF MS/MS and HPLC ESI MS/MS

In order to provide a proper amount of peptides for MS analysis, semi-preparative gels, containing 400 μg of total protein extract *per* strip, were loaded; electrophoretic conditions were the same as for 2-D DIGE, except that gels were stained with a protein fluorescent stain, as recommended by manufacturer (Deep Purple Total Protein Stain, 5mL/L, GE Healthcare). Images acquisition was performed using Typhoon 9200 laser scanner. Protein identification methods are provided below and in a MIAPE-MS compliant form in Supporting Information Table 1S [38]. Spots of interest were excised from gel using the Ettan spot picker robotic system (GE Healthcare), destained in 50% methanol/50 mM ammonium bicarbonate and incubated with 30 μL of 4 ng/μL trypsin (Promega) dissolved in 10 mM ammonium bicarbonate for 16 h at 37°C. Released peptides were subjected to reverse-phase chromatography (Zip-Tip C18 micro, Millipore), eluted with 50% ACN/1% formic acid. Briefly, 1 μL of peptides mixture was spotted onto the sample plate of an Ultraflex III MALDI-ToF/ToF (Bruker Daltonics) mass spectrometer; an equal volume of 10 mg/mL CHCA matrix dissolved in 70% ACN/30% 50 mM citric acid was applied and spots were air dried at room temperature. MS proceeded at an accelerating voltage of 25 kV and spectra were externally calibrated using Peptide Calibration Standard mixture (Bruker Daltonics); 1000 laser shots were taken *per* spectrum. Proteins were identified by comparing the digest peaks with a computer-generated database of tryptic peptides from known proteins using MASCOT, which utilizes a robust probabilistic scoring algorithm. Search was carried out by correlation of uninterpreted spectra to *Homo sapiens* entries in NCBInr Database. With regard to MASCOT parameters, one missed cleavage *per* peptide was allowed and carbamidomethylation, as fixed modification, and methionine oxidation, as variable modification, were set. Peptide mass tolerance was set at 30 ppm. In cases where this approach was unsuccessful, additional searches were performed using ESI-MS/MS. Tandem electrospray mass spectra were recorded using a Q-TOF mass spectrometer (Waters, Manchester, UK) interfaced to a Waters CapLC capillary chromatograph. Samples were dissolved in 0.1% aqueous formic acid, injected onto a 300 μm × 15 mm Pepmap C18 column (LC Packings, Amsterdam, The Netherlands), and eluted with an ACN/0.1% formic acid gradient. The capillary voltage was set to 3500 V. A survey scan over the m/z range of 400–1300 was used to identify protonated peptides with charge states of 2, 3 or 4, automatically selected for data-dependent MS/MS analysis, and fragmented by collision with argon. Signal-to-noise threshold value was set to 5. The resulting product ion spectra were transformed onto a singly charged m/z axis using a maximum entropy method (MaxEnt3, Waters), and the proteins were identified by correlation with uninterpreted spectra to entries in Swiss-Prot/TrEMBL, using ProteinLynx Global Server (Version 1.1, Waters). The database was created by merging the FASTA format files of Swiss-Prot, TrEMBL and their associated splice variants. No taxonomic, or protein mass, and p*I* constraints were applied. One missed cleavage *per* peptide was allowed, and the fragment ion mass tolerance window was set to 100 ppm. When identification was based on a single-matching peptide, the sequences were confirmed by manual sequencing using the MassLynx program PepSeq (Waters). Measured parent and fragment masses were typically within 0.03 Da of their calculated values.

2.4.6 MyHC isoform composition

SDS electrophoresis was performed on muscle extracts using a discontinuous buffer system with a 4% stacking gel (pH 6.8) and 37% glycerol, 6% T constant concentration running gel (pH 8.8) [46]. Samples were separated at 100 V, overnight. Gels were stained with SYPRO Orange (Molecular Probe) and scanned using a 570 nm emission filter on Typhoon 9200 Imager (GE Healthcare). Protein band quantification was achieved using Image Quant software (Molecular Dynamics); for each lane, MyHC bands were

normalized against the total MyHC content. Individual samples (1 μg) were run in triplicate. Molecular weight markers containing MyHC from rabbit (212 kDa) and bovine α2-macroglobulin (170 kDa) were run in a separate lane. Differences between controls and bed rest without and with countermeasures were computed by Student's *t*-test, the significance level being set at $p < 0.01$. A two-tailed *F*-test was applied in order to verify the homoscedasticity of variances. MyHC isoforms were gel excised and hydrolyzed by trypsin, as previously described, after reduction and alkylation of cysteine residues by 10 mM DTT (100 mL, 45 min at 56°C) and 55 mM iodoacetamide (100 mL, 30 min at room temperature in the dark), respectively. Proteins were identified by ESI-MS/MS.

2.4.7 MyLC isoform distribution

To semi-quantitate the MyLC isoforms distribution typical of slow and fast fibers, 50 μg of labelled protein extracts were separated in a 4.5–5.5 pH gradient in the first dimension, and the second dimension was performed as indicated above. Gel images were acquired by laser scanner and quantitated by DeCyder as described previously.

2.4.8 Immunoblotting

Protein extracts (50 μg), from samples analyzed by 2-D DIGE, were resolved by SDS-PAGE in triplicate and transferred at 300 mA for 180 min to PVDF membranes utilizing a Transblot Cell (GE Healthcare). The membranes were blocked in TBS (20 mM Tris, 137 mM NaCl, 0.1% Tween, pH 7.5) containing 5% fat-free milk powder. The membranes were incubated with antibodies diluted as follows: polyclonal anti-PGC-1α, 1:1000 as primary antibody (Santa Cruz Biotechnology, sc-13067, 200 μg/mL) and 1:10 000 peroxidase conjugate anti-rabbit as secondary antibody (GE Healthcare, NA934). Signals were visualized by chemiluminescence by ECL plus (GE Healthcare). The images were scanned and each band was quantitated using ImageQuant Software (GE Healthcare). The data were normalized against the total amount of proteins stained by Sypro Ruby and subjected to a Student's *t*-test and differences were considered significant at $p < 0.05$.

2.4.9 Bioinformatic data analysis

To examine and visualize ''canonical pathways'' of proteins regulated by the long immobilization without (BR) and with RVE countermeasures, the data were analyzed by using the IPA system (Ingenuity® Systems, www.ingenuity.com). This program uses a knowledge database derived from the literature to relate gene products (*e.g.* genes, mRNAs and proteins) based on their interactions and function. The Swiss-Prot accession numbers of differentially expressed proteins in VL and SOL after bed rest without and with RVE countermeasures were tabulated in Microsoft Excel and inserted into the program. Proteins matched to the corresponding gene objects in the Ingenuity Pathways Knowledge Base were named ''focus proteins''. The latter were then used as starting points through the database for interactions with other proteins stored in the database in order to generate ''canonical pathways''. The significance of the association between the data set and the ''canonical pathways'' was measured by calculating either: (i) the ratio of the number of proteins from the data set that map to the pathway with respect to the total number of proteins mapping to the ''canonical pathway''; (ii) the Fischer's exact test *p*-value ($p < 0.05$) determining the probability that the association between the proteins in the data set and the ''canonical pathway'' was explained by chance only.

3 Results

3.1 Physical and physiological characteristics of the subjects

The body mass of the subjects was essentially unchanged throughout the experiment. Maximum aerobic power could not be measured at the end of bed rest to avoid interference with the results of most concurrent programmed measurements. From the literature data, it appears that the consequences of 50–60 days of bed rest on VO_2 max are on the order of ~−20% [47].

During bed rest, the CSA of both VL and SOL underwent in BR conditions a decrement of ~15%. Maximum torque of both knee extensor and plantar flexor muscle groups decreased by ~22% [35]. Reduction of CSA and maximum torque was almost entirely prevented by RVE in both the investigated muscles. Fiber-type distribution was assessed pre- and post-55 days of bed rest by image scans after specific staining on cryosections [35]. No significant changes were detected after BR in VL, whereas RVE induced a significant ($p < 0.05$) shift from type I to type II. As for the SOL, a slight non significant shift of fiber types I–II was observed in BR that did not occur after RVE.

3.2 MyHC isoform composition of SOL and VL muscles after 55 days of bed rest with and without RVE countermeasures

In order to characterize muscles according to their MyHC isoforms' distribution, the latter not detectable by 2-D, SDS gel analysis and semi-quantitative assessment ($p < 0.01$) were carried out in both muscles before and after 55 days bed rest, without and with RVE countermeasures. The results are shown in Fig. 2. In VL after BR, an increment of type I (+5%) and of type IIX (+7%), and a decrement of

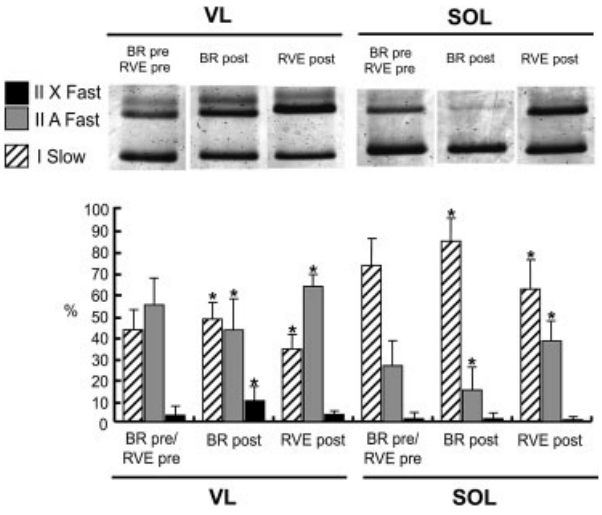

Figure 2. SDS-PAGE of protein extracts of VL and SOL before (pre-) and after (post-) bed rest without (BR) and with (RVE) exercise countermeasures. In total, 1 μg of proteins was loaded *per* lane. Graphical representation of MyHC fiber type composition (%) in all bed rest groups. Protein band quantification was performed by Image Quant (Molecular Dynamics) software. Differences were computed by Student's *t*-test, the significance level being set at $p<0.01$. A two-tailed *F*-test was applied in order to verify the homoscedasticity of variances. Significant differences are indicated by asterisks.

type IIA (−12%) isoforms were shown. Adopting RVE countermeasures induced a decrement of type I isoforms (−9%) and an increment of isoforms type IIA (+8%), whereas the switch to type IIX was absent. Isoform composition of SOL appeared even more affected by bed rest both without and with RVE countermeasures, bed rest being characterized by an increment of type I (+12%) isoforms and by a decrement of type IIA isoforms (−12%), whereas type IIX was not statistically changed. Countermeasures induced a marked decrement of type I isoforms (−11%) and an increment of type IIA isoforms (+11%). No changes were found for type IIX isoforms, as was the case for the VL. Detailed MS data of MyHC isoforms are summarized in Supporting Information Table 3S.

3.3 Detection and identification of proteins differentially expressed in the VL and the SOL muscles before and after bed rest

MyHC isoforms' distribution provides direct information on adjustments of contractile properties, and, indirectly, on metabolic adaptations. To define the relationship between the MyHC isoforms changes and the possible alteration of metabolic and regulatory proteins occurring in this peculiar model of immobilization, a comparative proteome analysis is required. To this purpose, a 2-D DIGE strategy was applied. Figure 3A shows a representative individual 2-D map of skeletal muscle proteome. Spots found differentially changed by in-gel differential analyses (post- *versus* pre-BR and post- *versus* pre-RVE) are indicated by spot numbers.

In VL muscle, 57 common spots were differentially expressed in each investigated subject (post- *versus* pre-BR, *t*-test: $p<0.05$), of which, 33 were identified by MS. For each spot, the statistical analysis (average ratio and *p*-values), the protein accession number, together with the molecular mass and p*I*, are listed in Table 2. Detailed MS data are summarized in Supporting Information Table 4S and shown in Supporting Information Fig. 3S. Among metabolic proteins, two isoforms of glycogen phosphorylase (muscle form) and of α-enolase were increased, suggesting an increment of the anaerobic metabolism. A decrement of mitochondrial proteins such as dihydrolipoil dehydrogenase, succinyl-CoA ligase, aconitate hydratase (three isoforms) and ubiquinol–cytochrome *c* reductase complex core protein I indicate a decrement of aerobic metabolism. Whereas galectin-1, a protein involved in cell cycle, and two isoforms of elongation factor 2 increase. The majority of transport carrier proteins were significantly reduced (apolipoprotein A-1 precursor, two isoforms of serum albumin and serotransferrin) with the exception of the voltage-dependent anion-selective channel protein 1 and myoglobin which were increased. Some proteins related to stress response were upregulated, whereas others were downregulated, suggesting a possible specific role of their modulation. Peroxiredoxin-2, HSPs β-6 and β-1 were less abundant, by contrast peroxiredoxin-6, peroxiredoxin-1, protein DJ-1, HSP 90-β, 78 kDa glucose-regulated protein and glutathione-*S*-transferase μ 2 were more abundant. Carbonic anhydrase 1 showed a strong downregulation, whereas the specific muscle isoform of carbonic anhydrase 3 was increased. As for contractile and structural proteins, WD repeat protein 1 (two isoforms) and vinculin were higher. Phosphatidylethanolamine-binding protein 1 was also more abundant.

With regard to the SOL, muscle differential analysis (post- *versus* pre-BR) indicates 47 spots statistically changed ($p<0.05$) common to all subjects, 26 of them identified by MS (Fig. 3A). For each spot, the statistical analysis (average ratio and *p*-values), the protein accession numbers, together with the molecular mass and p*I*, are listed in Table 3. Detailed MS data are summarized in Supporting Information Table 4S and shown in Supporting Information 3 Fig. 3S. Metabolic proteins were characterized by a slight increment of glycolytic enzyme α-enolase and glycogenin-1, accompanied by a marked decrement of proteins involved in aerobic metabolism such as succinyl-CoA ligase, aconitate hydratase (three isoforms), NADH dehydrogenase iron–sulfur protein 3 and ubiquinol–cytochrome *c* reductase complex core protein I. At variance with VL muscle, transport proteins, such as three isoforms of serum albumin, were markedly upregulated. Stress proteins showed larger differences compared with VL muscle. A common increased abundance was observed for peroxiredoxin-6 and 78 kDa

Table 2. *p*-Value of protein differentially expressed in human VL muscle after 55 days of immobilization without countermeasures (post- *versus* pre-) by paired Student's *t*-test

Functional classification	Spot number	Swiss-Prot accession number	Protein name	Paired Student's *t*-test *p*-value	Paired average ratio V_{V55}/V_{V2} (fold change)[a)]	Theoretical molecular mass (Da)	Theoretical p*I*
Structural proteins	32	O75083	WD repeat protein 1	2.20E–5	1.36	66 193.52	6.17
	33	O75083	WD repeat protein 1	0.015	1.32	66 193.52	6.17
	2	P18206	Vinculin	0.0045	1.73	123 799.3	5.5
Anaerobic metabolism	51	P06733	α-Enolase	0.0012	1.19	47 037.77	6.99
	10	P11217	Glycogen phosphorylase, muscle form	0.00075	1.55	96 960.86	6.57
	9	P11217	Glycogen phosphorylase, muscle form	0.049	1.34	96 960.86	6.57
Aerobic metabolism	38	P09622	Dihydrolipoyl dehydrogenase, mitochondrial [Precursor]	0.0097	−1.5	50 147.55	6.35
	46	P31930	Ubiquinol–cytochrome *c* reductase complex core protein I, mitochondrial [Precursor]	0.033	−1.23	49 128.6	5.43
	11	Q99798	Aconitate hydratase, mitochondrial [Precursor]	0.014	−1.48	82 425.78	6.85
	12	Q99798	Aconitate hydratase, mitochondrial [Precursor]	0.04	−1.47	82 425.78	6.85
	13	Q99798	Aconitate hydratase, mitochondrial [Precursor]	0.048	−1.34	82 425.78	6.85
	50	Q9P2R7	Succinyl-CoA ligase [ADP-forming] β-chain, mitochondrial [Precursor]	0.0037	−1.27	44 584.75	5.61
Transport proteins	90	P02144	Myoglobin	0.00043	1.36	17 183.81	7.14
	61	P21796	Voltage-dependent anion-selective channel protein 1	0.00061	1.17	30 772.6	8.62
	81	P02647	Apolipoprotein A-I [Precursor]	0.00012	−3.17	28 078.62	5.27
	29	P02768	Serum albumin [Precursor]	0.00042	−2.1	66 472.21	5.67
	28	P02768	Serum albumin [Precursor]	0.0011	−2.11	66 472.21	5.67
	16	P02787	Serotransferrin [Precursor]	5.20E−09	−2.35	75 181.44	6.7
Stress proteins and ROS scavenging proteins	74	P07451	Carbonic anhydrase 3	5.70E−05	1.43	29 426.23	6.94
	21	P08238	HSP 90-β	0.022	1.3	83 133.01	4.97
	23	P11021	78 kDa glucose-regulated protein [Precursor]	0.032	1.39	70 478.57	5.01
	78	P28161	Glutathione-*S*-transferase μ 2	0.0031	1.57	25 613.46	6.02
	77	P30041	Peroxiredoxin-6	0.0027	1.29	24 903.79	6.02
	89	Q06830	Peroxiredoxin-1	0.0029	1.28	22 110.36	8.27
	80	Q99497	Protein DJ-1	5.20E−06	1.22	19 891.05	6.33
	86	O14558	HSP β-6	0.032	−1.56	17 135.6	5.95
	73	P00915	Carbonic anhydrase 1	0.0041	−2.45	28 739.02	6.63
	87	P04792	HSP β-1	0.0076	−1.52	22 782.52	5.98
	83	P32119	Peroxiredoxin-2	0.0068	−1.55	21 760.73	5.67
Protein synthesis	7	P13639	Elongation factor 2	0.024	1.28	95 206.95	6.42
	8	P13639	Elongation factor 2	7.80E−08	1.37	95 206.95	6.42
Cell cycle	92	P09382	Galectin-1	0.02	1.42	14 584.51	5.34
Other	88	P30086	Phosphatidylethanolamine-binding protein 1	0.0011	1.33	20 925.59	7.43

a) V_{V55}/V_{V2} indicates the value derived from the normalized spot volume standardized against the intra-gel standard provided by DeCyder software analysis.

glucose-related protein (two isoforms), whereas a decrement of HSP β-1 was profiled. In addition, a peculiar increment of proteins involved in mitochondrial ROS production such as glutathione-*S*-transferase μ 2, glutathione transferase ω-1, protein disulfide-isomerase A3 was observed. Significant changes were found in structural and contractile proteins, particularly, an increased abundance of gelsolin and vinculin. The latter were accompanied by a decrement of Kelch repeat and BTB domain-containing protein 10 (two isoforms), actin γ-enteric smooth muscle, actin α cardiac muscle 1 and mitochondrial inner membrane protein (two isoforms).

3.4 Effects of RVE countermeasures on protein differential expression

In VL, RVE countermeasures applied during bed rest (post-*versus* pre-RVE), induced ubiquitous individual changes in 30 spots, 26 of them identified by MS as shown and summarized in Fig. 3A and Table 4. MS data are summarized in Supporting Information Table 4S and shown in Supporting Information in Fig. 3S. Increment of metabolic proteins related to carbohydrate metabolism, Krebs cycle, mitochondrial respiratory chain and lipid metabolism was observed. Dihydrolipoil dehydrogenase, 3-hydroxyisobutyrate dehydrogenase, 2-oxoglutarate dehydrogenase E1 component (four isoforms), aconitate hydratase (two isoforms), ubiquinol–cytochrome *c* reductase complex core protein 1, ATP synthase D chain, very long chain-specific acyl-CoA dehydrogenase mitochondrial, enoyl-CoA hydratase mitochondrial and 3,2-trans-enoyl-CoA isomerase were increased. Stress-related proteins, thioredoxin-dependent peroxide reductase, 60 kDa HSP mitochondrial, protein disulfide-isomerase A3 and heat shock-related 70 kDa protein 2 were more abundant, whereas HSP β-1 decreased.

RVE countermeasures during bed rest induced in the SOL of all subjects significant abundance changes in 50 spots, 41 of them identified by MS as shown and summarized in Fig. 3A and Table 5. MS data are summarized in Supporting Information Table 4S and shown in Supporting Information Fig. 3S. As previously observed for SOL after BR, an increment of proteins involved in carbohydrate, gluconeogenesis and glucose metabolisms was observed. Proteins such as glyceraldehyde-3-phosphate dehydrogenase

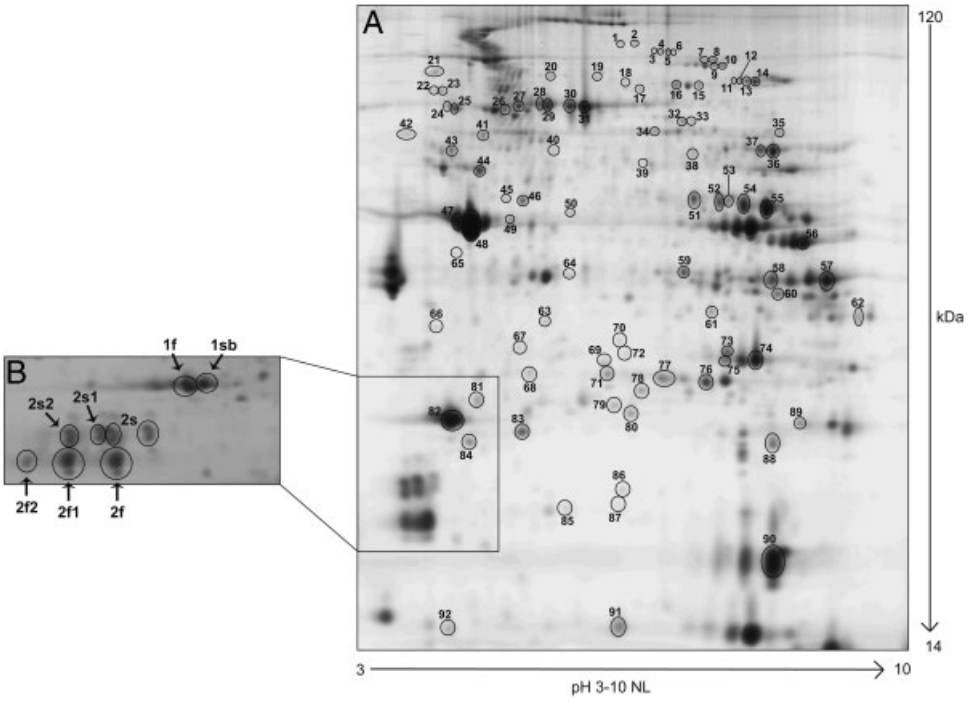

Figure 3. (A) Skeletal muscle protein profiling by 2-D DIGE. A representative individual 2-D pattern gel image of 40 μg of protein extract, separated in a pH 3–10 non-linear IPG strip in the first dimension and SDS gel (12% T, 2.5% C) as the second dimension. The image was acquired with a 532 nm laser beam and 580 nm emission filter. Automated image analysis by DeCyder software detected and matched 3000 protein spots in a single-gel image. Spots found differentially changed by in-gel differential analysis (post- *versus* pre-BR and post-*versus* pre-RVE, from VL and SOL) are indicated by spot number and listed in Tables 2–5. (B) Close-up of isoforms distribution of alkali MyLCs (MyLC1) slow (1sb) and fast (1f) and of myosin regulatory light chain 2 (MyLC2) slow (2s2, 2s1, 2s) and fast (2f2, 2f1, 2f) shown as close-up insertion from larger 2-D gel. Briefly, 50 μg of labelled protein extracts from pre- and post-BR and pre- and post-RVE from both muscles, VL and SOL, were separated in a pH 4.5–5.5 IPG strip in the first dimension and SDS gel (12% T, 2.5% C) in a second dimension. Gel images were acquired by laser scanner and analyzed by DeCyder software.

Table 3. *p*-Value of protein differentially expressed in human SOL muscle after 55 days of immobilization without countermeasures (post- *versus* pre-) by paired Student's *t*-test

Functional classification	Spot number	Swiss-Prot accession number	Protein name	Paired Student's *t*-test *p*-value	Paired average ratio V_{S55}/V_{S2} (fold change)[a)]	Theoretical molecular mass (Da)	Theoretical p*I*
Structural proteins	20	P06396	Gelsolin [Precursor]	0.00017	2.17	80 640.61	5.58
	1	P18206	Vinculin	0.0051	1.24	123 799.3	5.5
	24	O60662	Kelch repeat and BTB domain-containing protein 10	0.00088	−1.17	68 037.23	5.14
	25	O60662	Kelch repeat and BTB domain-containing protein 10	0.0041	−1.19	68 037.23	5.14
	18	Q16891	Mitochondrial inner membrane protein	0.00011	−1.32	83 677.91	6.08
	17	Q16891	Mitochondrial inner membrane protein	0.0011	−1.35	83 677.91	6.08
Contractile proteins	66	P63267	Actin, γ-enteric smooth muscle	0.016	−1.4	41 642.54	5.31
	48	P68032	Actin, α cardiac muscle 1	0.034	−1.22	42 018.97	5.23
Anaerobic metabolism	51	P06733	α-Enolase	0.02	1.2	47 037.77	6.99
	65	P46976	Glycogenin-1	0.00046	1.22	39 383.78	5.27
Aerobic metabolism	68	O75489	NADH dehydrogenase [ubiquinone] iron–sulfur protein 3, mitochondrial [Precursor]	0.0041	−1.31	26 414.92	5.48
	45	P31930	Ubiquinol–cytochrome *c* reductase complex core protein I, mitochondrial [Precursor]	0.028	−1.22	49 128.6	5.43
	12	Q99798	Aconitate hydratase, mitochondrial [Precursor]	0.0037	−1.28	82 425.78	6.85
	13	Q99798	Aconitate hydratase, mitochondrial [Precursor]	0.03	−1.25	82 425.78	6.85
	14	Q99798	Aconitate hydratase, mitochondrial [Precursor]	0.032	−1.22	82 425.78	6.85
	50	Q9P2R7	Succinyl-CoA ligase [ADP-forming] β-chain, mitochondrial [Precursor]	0.0096	−1.38	44 584.75	5.61
Transport proteins	28	P02768	Serum albumin [Precursor]	0.015	1.55	66 472.21	5.67
	29	P02768	Serum albumin [Precursor]	0.02	1.6	66 472.21	5.67
	30	P02768	Serum albumin [Precursor]	0.044	1.61	66 472.21	5.67
Stress proteins and ROS scavenging proteins	22	P11021	78 kDa glucose-regulated protein [Precursor]	0.00061	1.26	70 478.57	5.01
	23	P11021	78 kDa glucose-regulated protein [Precursor]	0.0069	1.25	70 478.57	5.01
	78	P28161	Glutathione-*S*-transferase μ 2	0.028	1.41	25 613.46	6.02
	77	P30041	Peroxiredoxin-6	0.013	1.24	24 903.79	6.02
	40	P30101	Protein disulfide-isomerase A3 [Precursor]	0.0015	1.62	54 265.22	5.61
	70	P78417	Glutathione transferase ω-1	0.022	1.43	27 565.86	6.24
	85	P04792	HSP β-1	6.70E−05	−1.66	22 782.52	5.98

a) V_{S55}/V_{S2} indicates the value derived from the normalized spot volume standardized against the intra-gel standard provided by DeCyder software analysis.

Table 4. *p*-Value of protein differentially expressed in human VL muscle after 55 days of immobilization with countermeasures (post- *versus* pre-) by paired Student's *t*-test

Functional classification	Spot number	Swiss-Prot accession number	Protein name	Paired Student's *t*-test *p*-value	Paired average ratio V_{V55}/V_{V2} (fold change)[a)]	Theoretical molecular mass (Da)	Theoretical p*I*
Structural proteins	2	P18206	Vinculin	0.00017	1.23	123 799.3	5.5
	18	Q16891	Mitochondrial inner membrane protein	0.0032	1.45	83 677.91	6.08
	19	Q16891	Mitochondrial inner membrane protein	0.0034	1.29	83 677.91	6.08
	62	O75112	LIM domain-binding protein 3	0.033	−1.18	35 637.17	9.69
	60	Q9NP98	Myozenin-1	0.025	−1.35	31 744.65	8.86
Contractile proteins	66	P63267	Actin, γ-enteric smooth muscle	0.037	−1.29	41 642.54	5.31
	47	P68032	Actin, α cardiac muscle 1	0.0011	−1.27	42 018.97	5.23
Aerobic metabolism	84	O75947	ATP synthase D chain, mitochondrial	0.0063	1.35	18 491.21	5.21
	38	P09622	Dihydrolipoyl dehydrogenase, mitochondrial [Precursor]	8.00E−08	1.38	50 147.55	6.35
	69	P30084	Enoyl-CoA hydratase, mitochondrial [Precursor]	0.0063	1.3	28 342.6	5.88
	46	P31930	Ubiquinol–cytochrome *c* reductase complex core protein 1, mitochondrial [Precursor]	0.014	1.39	49 128.6	5.43
	63	P31937	3-Hydroxyisobutyrate dehydrogenase, mitochondrial [Precursor]	0.017	1.33	31 537.41	5.54
	72	P42126	3,2-Trans-enoyl-CoA isomerase, mitochondrial [Precursor]	0.0069	1.31	28 736.19	6
	35	P49748	Very long chain-specific acyl-CoA dehydrogenase, mitochondrial [Precursor]	0.043	1.41	66 175.14	7.74
	6	Q02218	2-Oxoglutarate dehydrogenase E1 component, mitochondrial [Precursor]	0.0018	1.41	111 339.89	6.07
	5	Q02218	2-Oxoglutarate dehydrogenase E1 component, mitochondrial [Precursor]	0.0021	1.43	111 339.89	6.07
	3	Q02218	2-Oxoglutarate dehydrogenase E1 component, mitochondrial [Precursor]	0.0086	1.2	111 339.89	6.07
	4	Q02218	2-Oxoglutarate dehydrogenase E1 component, mitochondrial [Precursor]	0.0099	1.37	111 339.89	6.07
	14	Q99798	Aconitate hydratase, mitochondrial [Precursor]	0.0052	1.39	82 425.78	6.85
	13	Q99798	Aconitate hydratase, mitochondrial [Precursor]	0.029	1.21	82 425.78	6.85
Stress proteins and ROS scavenging proteins	41	P10809	60 kDa HSP, mitochondrial [Precursor]	0.0055	1.25	57 962.86	5.24
	79	P30048	Thioredoxin-dependent peroxide reductase, mitochondrial [Precursor]	0.0088	1.25	21 468.45	5.77
	40	P30101	Protein disulfide-isomerase A3 [Precursor]	0.034	1.23	54 265.22	5.61
	27	P54652	Heat shock-related 70 kDa protein 2	0.0039	1.2	70 020.97	5.56
	71	P04792	HSP β-1	0.004	−1.38	22 782.52	5.98
Cell cycle	67	P35232	Prohibitin	0.0063	1.23	29 804.1	5.57

a) V_{V55}/V_{V2} indicates the value derived from the normalized spot volume standardized against the intra-gel standard provided by DeCyder software analysis.

Table 5. *p*-Value of protein differentially expressed in human SOL muscle after 55 days of immobilization with countermeasures (post- *versus* pre-) by paired Student's *t*-test

Functional classification	Spot number	Swiss-Prot accession number	Protein name	Paired Student's *t*-test *p*-value	Paired average ratio V_{S55}/V_{S2} (fold change)[a)]	Theoretical molecular mass (Da)	Theoretical p*I*
Structural proteins	32	O75083	WD repeat protein 1	6.20E−05	1.5	66 193.52	6.17
	33	O75083	WD repeat protein 1	0.0048	1.43	66 193.52	6.17
	20	P06396	Gelsolin [Precursor]	0.0034	1.69	80 640.61	5.58
	44	P17661	Desmin	0.028	1.35	53 535.79	5.21
	2	P18206	Vinculin	0.017	1.34	123 799.3	5.5
	43	P68366	Tubulin α-1 chain	0.00024	1.49	49 924.4	4.95
	19	Q16891	Mitochondrial inner membrane protein	0.034	1.36	83 677.91	6.08
	64	Q9P100	LIM-only protein FHL3 (four and a half LIM domains 3)	0.0081	−1.28	31 282.09	5.79
Contractile proteins	59	P45378	Troponin T, fast skeletal muscle	0.025	3.32	31 824.55	5.71
	82	P05976	Myosin light chain 1, skeletal muscle isoform	0.0073	−1.43	21 145.11	4.97
	66	P63267	Actin, γ-enteric smooth muscle	0.023	−1.5	41 642.54	5.31
	49	P68133	Actin, α skeletal muscle	0.018	−1.31	42 051.03	5.23
Aerobic metabolism	56	P04075	Fructose-bisphosphate aldolase A	0.028	1.4	39 288.83	8.39
	58	P04406	Glyceraldehyde-3-phosphate dehydrogenase	0.017	1.81	35 922.02	8.58
	57	P04406	Glyceraldehyde-3-phosphate dehydrogenase	0.018	1.55	35 922.02	8.58
	51	P06733	α-Enolase	0.023	1.19	47 037.77	6.99
	9	P11217	Glycogen phosphorylase, muscle form	0.021	1.37	96 960.86	6.57
	54	P13929	β-Enolase	0.0012	1.72	46 855.69	7.73
	52	P13929	β-Enolase	0.0025	1.53	46 855.69	7.73
	55	P13929	β-Enolase	0.0056	1.69	46 855.69	7.73
	53	P13929	β-Enolase	0.013	1.28	46 855.69	7.73
	37	P14618	Pyruvate kinase isozymes M1/M2	0.0026	1.43	57 805.7	7.95
	36	P14618	Pyruvate kinase isozymes M1/M2	0.0027	1.57	57 805.7	7.95
	34	P36871	Phosphoglucomutase-1	0.0003	2.73	61 317.93	6.32
	76	P60174	Triosephosphate isomerase	0.0088	1.45	26 538.3	6.51
	45	P31930	Ubiquinol–cytochrome *c* reductase complex core protein 1, mitochondrial [Precursor]	0.038	−1.26	49 128.6	5.43
Transport proteins	31	P02768	Serum albumin [Precursor]	0.03	1.77	66 472.21	5.67
	15	P02787	Serotransferrin [Precursor]	0.021	2.36	75 181.44	6.7
	91	P05413	Fatty acid-binding protein, heart	0.038	−1.47	14 726.84	6.34
Stress proteins and ROS scavenging proteins	71	P04792	HSP β-1	0.004	1.37	22 782.52	5.98
	42	P07237	Protein disulfide-isomerase [Precursor]	0.011	1.63	55 294.02	4.69
	75	P07451	Carbonic anhydrase 3	0.035	1.66	29 426.23	6.94
	74	P07451	Carbonic anhydrase 3	0.036	2	29 426.23	6.94
	26	P11142	Heat shock cognate 71 kDa protein	0.0055	1.41	70 766.9	5.37
	40	P30101	Protein disulfide-isomerase A3 [Precursor]	0.003	1.51	54 265.22	5.61
	27	P54652	Heat shock-related 70 kDa protein 2	0.023	1.3	70 020.97	5.56

Table 5. Continued

Functional classification	Spot number	Swiss-Prot accession number	Protein name	Paired Student's *t*-test *p*-value	Paired average ratio V_{S55}/V_{S2} (fold change)[a)]	Theoretical molecular mass (Da)	Theoretical p*I*
	39	P78371	T-complex protein 1 subunit β (chaperonin containing TCP1, subunit 2 (β))	0.048	1.28	57 357.02	6.02
	70	P78417	Glutathione transferase ω-1	0.045	−1.35	27 565.86	6.24
Protein synthesis	8	P13639	Elongation factor 2	0.046	1.38	95 206.95	6.42
Cell cycle	92	P09382	Galectin-1	0.0043	1.77	14 584.51	5.34
	67	P35232	Prohibitin	0.00022	−1.23	29 804.1	5.57

a) V_{S55}/V_{S2} indicates the value derived from the normalized spot volume standardized against the intra-gel standard provided by DeCyder software analysis.

(two isoforms), α-enolase, β-enolase (four isoforms), glycogen phosphorylase muscle form, fructose-bisphosphate aldolase A, phosphoglucomutase-1, pyruvate kinase isozymes M1/M2 (two isoforms) and triosephosphate isomerase were upregulated. Low abundance of some key enzymes of the respiratory chain was detected such as prohibitin and ubiquinol–cytochrome *c* reductase complex core protein 1. Proteins involved in cell cycle, such as galectin-1 and in protein translation and synthesis, such as elongation factor 2 were increased. The abundance of proteins involved in ROS production showed a peculiar behaviour most of them being upregulated such as HSP β-1, heat shock cognate 71 kDa protein, heat shock-related 70 kDa protein 2, protein disulfide-isomerase and subunit A3, T-complex protein 1 subunit β, whereas glutathione transferase ω-1 was decreased. Structural and contractile proteins abundance assessment indicated a decrement of MyLC1, actin γ-enteric smooth muscle and α skeletal muscle, LIM domain 3, whereas WD repeat protein 1 (two isoforms), gelsolin, desmin, vinculin, tubulin α-1 chain, mitochondrial inner membrane protein and troponin T fast were increased. Transport proteins were also altered: serum albumin and serotransferrin were increased, whereas fatty acid-binding protein was decreased. As for carbonic anhydrase 3, both isoforms were more abundant and may play a role in regulating the acid–base balance of the muscle and, particularly, protect the fibrocell from oxidative damage [48].

3.5 MyLC in the VL and in the SOL without and with RVE countermeasures

A detailed analysis of MyLC light chain isoforms was performed in a narrow pH gradient, as first dimension, in order to detect possible changes in distribution, particularly of isoforms functionally relevant for force development, such as the phosphorylatable acidic subunits. A gel close up is shown in Fig. 3B. The isoforms were labelled according to the literature as shown in the legend. Quantitative analysis indicates that no changes in MyLC isoforms distribution were induced by immobilization without (BR) and with RVE countermeasures in VL. On the contrary, a decrement of the non-phosphorylatable isoforms MyLC 1a and MyLC 2f was observed in SOL after RVE countermeasures (data not shown).

3.6 The role of PGC-1α in the muscle catabolic state

To gain insight into the relationship between protein abundance and muscle energy balance, PGC-1α was assessed by immunoblotting on muscle extracts before and after bed rest, without and with RVE countermeasures. As shown in Fig. 4, PGC-1α levels were not significantly influenced in either condition in VL. In SOL, no changes were observed after BR, whereas RVE induced a statistically significant increase.

3.7 A bioinformatic treatment of the results by IPA

In an attempt to get further insight into the functional significance of the data, a bioinformatic analysis of the differentially expressed proteins was carried out adopting IPA. On the basis of the system criteria, 64 differently abundant proteins were involved in the identified networks. Five so-called ''canonical pathways'' were selected over the significance threshold (−log (*p*-value) = 1.3) (Fig. 5). These were mitochondrial dysfunction which was over-represented in both VL and SOL (without and with RVE countermeasures); fatty acid metabolism, which was over-represented in VL; oxidative stress under Nrf2 control over-represented in all categories, stress response over-represented both in VL and in SOL without and with RVE countermeasures; aryl hydrocarbon receptor (AHR) signalling which was over-represented in both VL and SOL without RVE countermeasures; negative acute-phase response, over-represented in all conditions. The analysis supports the hypothesized ''canonical pathways'', introducing an over-representation of the negative acute-phase response and AHR signalling. In addition, it also provides evidence of a substantial influence of RVE countermeasures, particularly in SOL in BR.

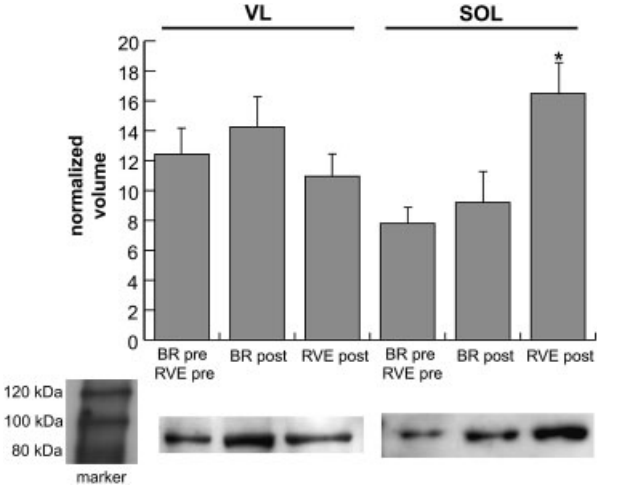

Figure 4. PGC-1α quantitation by immunoblotting. Protein extract (50 μg), from the individual samples analyzed by 2-D DIGE, was separated in 6% SDS-PAGE gel and electrotransferred to PVDF membrane. A polyclonal anti-PGC-1α (1:1000 dilution) and an anti-rabbit peroxidase conjugate (1:10 000) antibodies were utilized. The signals were revealed by ECL Plus. The histogram represents the mean values for volumes calculated for each detected band using the ImageQuant Software. Differences were computed by Student's *t*-test, the significance level being set at $p < 0.05$. Significant differences are indicated by asterisks.

4 Discussion

In this study, structural and functional changes combined with proteome analysis enabled us to describe and explain specific alterations in response to bed rest without and with RVE countermeasures. Concerning proteomic analyses, it should be pointed out that, due to the study design, BR and RVE data are the outcome of two separate and independent investigations. This procedure, depending on the adopted statistical data treatment (paired Student's *t*-test), limits further potential information. This approach is novel in human muscle research and presents several advantages over previous investigations. In fact, this study: (i) is the first proteomic characterization of two metabolically different muscles in the same subject that are differently influenced by bed rest; (ii) features changes induced by RVE countermeasures in muscles with different fiber types composition. Moreover, by analyzing the above-described results with bioinformatic tools, it was possible to demonstrate the existence of bed rest-induced catabolic pathways, thereby shedding light on the changes brought about by immobilization and the strategy elicited by RVE to counteract the atrophic process in healthy male subjects. A gene expression profile analysis yielding a list of perturbed genes grouped in molecular networks and biological processes has been recently obtained for the same muscles in females during 60 days of

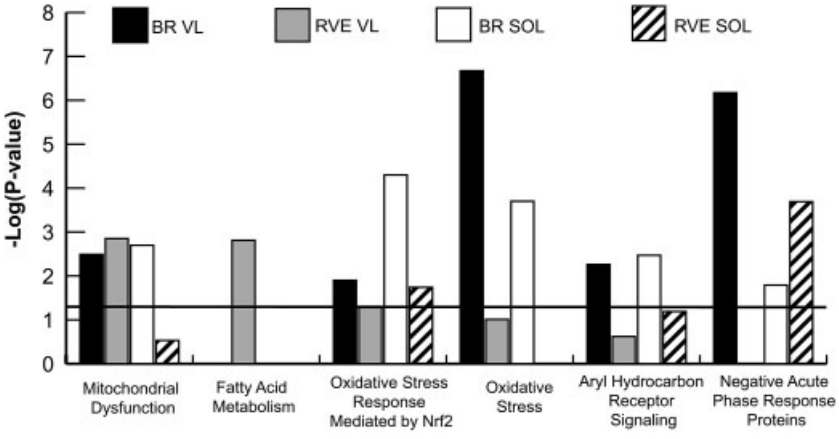

Figure 5. Altered functions in VL and SOL during bed rest without and with RVE countermeasure identified by IPA software. The functional groups are displayed along the *x*-axis. The *y*-axis displays the −log-(significance) of the functional groups. Functions are listed from the most significant to the least significant ones and the black line indicates the threshold of significance ($p = 0.05$).

bed rest without and with exercise countermeasures and/or dietary protein supplementation (WISE study 2005) [49].

4.1 Morphometric parameters

Body mass and physical performance parameters of the investigated subjects are in agreement with those observed in the previous bed rest studies. The observed reduction of muscle cross section after 55 days of BR is well within the range of the literature data for both quadriceps and calf muscle after a comparable period of BR immobilization. The corresponding decrease of knee extensor and plantar flexor maximum torque, respectively, is also within the range of the values found by others in comparable experimental conditions [50], (Ferretti 2009, personal communication). For a functional evaluation of the investigated muscles, it was assumed that the above figures would apply uniformly to each of the VL heads and to the whole SOL, respectively. In any case, it is worth noting that our findings are characterized by a high inter-individual variability. RVE countermeasures, according to the protocol adopted for this study whereby the subject underwent activation of both type I (aerobic) and type IIA and IIX (fast oxidative and glycolytic) fibers, were very effective in protecting average CSA and maximum torque of both VL and SOL muscles. The exercise metabolic load imposed by the RVE protocol can be inferred by the relatively high blood lactate levels (7–9 mM) incurred by the subjects after all-out squats exercise bouts of only 6 min duration throughout bed rest [37].

4.2 Fiber type switching during bed rest without and with countermeasures

In order to precisely profile MyHC distribution in VL and SOL, an electrophoretic technique suitable to detect fine adjustments evaluating semi-quantitatively, the various fractions of type I, IIA, IIX isoforms was adopted. The pattern of MyHC distribution (Fig. 2) appears to be affected by BR in both VL and SOL. MyHC IIA fibers, *i.e.* those characterized by both oxidative and glycolytic metabolism were particularly affected. In VL, this fiber fraction was partially split into slow oxidative type I and pure fast glycolytic type IIX fibers. RVE countermeasures were effective in counteracting this switch by lowering type I MyHC fraction thereby increasing the fibers with mixed phenotype, whereas MyHC IIX isoforms were unchanged. A postural muscle such as SOL, known to be largely influenced by BR, underwent a switch toward oxidative metabolism by RVE countermeasures featuring an increment of the mixed phenotype. The results obtained by electrophoresis of MyHC proteins are supported by immunohistochemical MyHC expression profiles previously reported from the same bed rest study [35]. Fiber type functional changes, particularly decrease of P_o and increase of V_o were described in humans after immobilization [13]. In a previous human muscle proteomic study of ageing [31], we suggested a possible dependence of muscle P_o and V_o on the level of acidic phosphorylatable isoforms fast (f) of MyLC. As shown in Fig. 3B, this correlation does not seem to occur during BR, a condition characterized by the absence of changes in MyLC phosphorylatable isoform distribution. With regard to metabolic proteins, during BR, there appears to be a progressive impairment of the oxidative pathway which, both in VL and in SOL, is partially prevented by the adopted protocol of RVE countermeasures. It appears that even very short lasting exercise bouts as those imposed by the present protocol can be very effective, provided an increase in aerobic metabolic rate above the anaerobic threshold is elicited together with a consistent accumulation of lactate in the exercised muscles, particularly in VL.

On the other hand, the relationships between the level of PGC-1α, the master regulator of mitochondrial biogenesis, atrogens program and of the metabolic changes characterizing a loss of muscle mass, occur particularly in SOL with RVE countermeasures. PGC-1α parallels in SOL after RVE the observed changes in MyHC isoforms' distribution and the upregulation in aerobic metabolism profiled by 2-D DIGE by way of increased mitochondrial activity.

4.3 Structural protein changes

Molecular changes occurring in the investigated muscles during bed rest at the structural level involving contractile proteins seem to be dominated by the mechanical stress imposed by muscle unloading and reloading without and with RVE countermeasures. A peculiar signature of mechanical stress sensors is profiled by the present proteome analysis. Indeed, some of the contractile proteins involved in mechanical stress [51] were deregulated, particularly in VL with RVE countermeasures. The above changes involve MyHCs, cardiac and skeletal actins, troponin subunits, LIM domain and myozenin. This functional impairment could profoundly influence the calcium-activated signalling process associated with the Z-disk function. It is known that the above mechanism involves molecules such as LIM domain proteins, PDZ-LIM domain proteins, myozenin gene family members, titin-associated ankyrin repeat family proteins, as well as muscle-specific ring finger proteins, which have been identified as potential molecular mechanical sensor components. An unequivocally significant role of calcium signalling is played by myozenin which was identified in skeletal muscle as a filamin-, actinin- and telethonin-binding protein at the Z-disk [52]. Among others, the organization of the thin filament also appears to be influenced by BR: the end-capping protein gelsolin increased during BR, whereas troponin T was found to be less abundant, suggesting that the single regulatory units of

the thin filament were also perturbed [53]. RVE countermeasures appear to counteract this alteration by increasing troponin T and gelsolin. The disruption of the sarcomeric organization could also be the consequence of a loss of titin, as observed in animal models [54] that was not detectable by the present analysis.

Mechanical stress sensors are not limited to the Z-disk region. They are also embedded in muscle-specific membrane systems such as the costamere, intercalated disks and caveolae-like microdomains (vinculin, desmin and WD repeat). The present analysis confirms that such modulation of muscle functions requires an integrated analysis to determine the molecular events profiling functional changes. In any case, the stressor elements are induced by RVE that appear to positively counteract the loss of sarcomeric organization found after BR.

4.4 Mitochondrial dysfunction

Mitochondria contain a series of redox carriers transferring single electrons to oxygen. Conditions of both lack of O_2 or hyperoxia but also bed rest, particularly when adopting RVE countermeasures [55], result in the generation of an excess of ROS particularly, superoxide. Mitochondria also contain an extensive antioxidant defense against ROS, which would otherwise cause oxidative damage to cellular components. This condition appears to occur during muscle inactivity such as during bed rest, particularly in the presence of RVE countermeasures.

Strictly related to mitochondrial defense is the dysregulation of a number of stress–response molecules such as *e.g.* glutathione-*S*-transferase μ 2, HSP 90-β, peroxiredoxin-1, glutathione-*S*-transferase ω 2, superoxide dismutase [Cu-Zn], actin γ-enteric smooth muscle, actin α cardiac muscle 1 and actin α skeletal muscle. These changes are under Nrf2 control. Nrf2 activates the antioxidant machinery and suppresses proinflammatory pathways mediated by NF-κB signalling [56]. The overexpression of this set of molecules indicates that BR is a stressful condition and induces changes, leading to a loss of muscle mass and function. RVE appears to counteract these events only partially, and it is difficult to assess if the adopted protocol aimed at counteracting muscle loss is the most appropriate to restore muscle function. In this context, it is noteworthy that carbonic anhydrase 1, which is inhibited by nitric oxide signals [57], remains strongly downregulated at least in VL, a finding that could indirectly reflect iNOS induction. Heat shock factor 1, which is essential for protecting cells from protein-damage associated with misfolded proteins and which regulates the insulin-signaling pathway during aging [58], is also less abundant following BR and was even not restored to a physiological level in VL with RVE countermeasures. On the whole, the present findings, therefore, indicate a series of candidate molecules able to monitor and profile the effects of unloading and exercise countermeasure protocols in human skeletal muscles.

4.5 AHR signalling

The bioinformatic (IPA) approach also indicates activation of the AHR. The latter is a cytosolic protein associated with chaperone and immunophilin-like proteins (such as HSP90). Upon ligand activation, AHR dissociates from the complex, translocates into the nucleus and recruits several molecules for its further activation. This AHR complex induces transcriptional activation of genes encoding xenobiotic metabolizing enzymes (GST, NADPH-quinone oxidoreductase and UDP-glucuronyl-*S*-transferase) and other growth factors and proteins, involved in cell-cycle progression and apoptosis. These events could be mediated by calcium-activated signaling, in particular *via* calcineurin whose modulation induces nuclear transcription. The induction of metabolic enzymes and, possibly, of post-transductional modifications directly and indirectly observed during BR shall put forward new hypotheses on the events related to BR-induced muscle waste and on the efficacy of exercise countermeasures.

4.6 Negative acute-response phase

With regard to the negative acute-response phase mediated by NF-κB signalling, the activation of this pathway supports the possible role of a mechanical stress response. The activation of this pathway, actually, is currently detected in muscle proteomic studies, particularly under pathological conditions [59]. Further investigation with different bed rest protocols is required to validate the present findings on unloaded and reloaded muscles.

4.7 Conclusions

Differential protein profiling during bed rest, particularly the study of muscle proteome changes attributable to exercise countermeasures, has proven to be an invaluable tool for the analysis of structural as well as metabolic changes occurring throughout lower limbs immobilization. It goes without saying that a 55-day post- *versus* pre-exposure comparison, as was the case for this study, does not allow to detect the time course of either anabolic or catabolic muscle protein balance. In fact, the latter is a biphasic process whereby an early decrease of protein synthesis accompanied by a downregulation of the pathways controlling muscle hypertrophy precedes the tissue degradation phase. Despite this limitation, the comparison of the metabolic dysregulation induced in two anatomically and functionally different muscles, such as the VL and the SOL, by vibration countermeasures, such as those adopted for the present investigation, provides unique information on both muscle protein signature in the course of BR, opening new avenues on protein variants as possible markers of rehabilitation and of monitoring of RVE countermeasures. The present data also

provide evidence of changes induced in SOL by the transcriptional coactivator PGC-1α known to effect fiber type switching from glycolytic toward oxidative. In addition, key protein analyses at appropriate time intervals throughout bed rest together with those monitoring the state of activation of metabolic pathways and of specific markers, particularly those related to mechanical stress and ROS control, shall prove extremely useful for the evaluation of the functional status of unloaded limb muscles throughout bed rest without and with exercise countermeasures.

It should be pointed out that muscle proteome analysis comprises (i) the characterization of all proteins expressed by the tissue and (ii) possible differences in protein abundance induced by physiological, paraphysiological and patological variables. In healthy subjects, the first published systematic characterization of the human VL muscle (by 2-DE-HPLC ESI-MS/MS) carried out in our laboratory dates back to year 2003 [60]. In 2008, Hojlund *et al.* characterized the same muscle by 1-D gel electrophoresis and HPLC ESI-MS/MS, providing a larger data set of proteins [61]. Subsequently, Kovalyova *et al.* identified 89 proteins in human VL by 2-DE and MALDI-ToF [62]. The above study is essentially descriptive and does not address any specific aspect of muscle function. More recently, Holloway *et al.* by using iTRAQ and 2-DE coupled with LC MALDI MS/MS investigated differential expression of metabolic and myofibrillar proteins in response to interval exercise training [63].

In conclusion, muscle proteomic profiling as carried out in healthy subjects during inactivity without and with exercise countermeasures provides a precise description of the functional status of the tissue. In addition, the analysis of the characteristics of negative and positive stimuli, such as training and detraining on muscle function, as well as of those aimed at post-traumatic rehabilitation or at the prevention of physiological and pathological sarcopenia, such as in ageing or in disease, could take advantage of the present approach.

This work has been funded by Agenzia Spaziale Italiana (ASI) to P. C. and Italian Ministry of University and Scientific Research (Grant: FIRB RBR NO7BMCT to C. G.).

The authors have declared no conflict of interest.

5 References

[1] Pavy-Le Traon, A., Heer, M., Narici, M. V., Rittweger, J., Vernikos, J., From space to Earth: advances in human physiology from 20 years of bed rest studies (1986-2006). *Eur. J. Appl. Physiol.* 2007, *101*, 143–194.

[2] LeBlanc, A. D., Schneider, V. S., Evans, H. J., Pientok, C. *et al.*, Regional changes in muscle mass following 17 weeks of bed rest. *J. Appl. Physiol.* 1992, *73*, 2172–2178.

[3] Widrick, J. J., Norenberg, K. M., Romatowski, J. G., Blaser, C. A. *et al.*, Force-velocity-power and force-pCa relationships of human soleus fibers after 17 days of bed rest. *J. Appl. Physiol.* 1998, *85*, 1949–1956.

[4] LeBlanc, A., Rowe, R., Evans, H., West, S. *et al.*, Muscle atrophy during long duration bed rest. *Int. J. Sports Med.* 1997, *18*, S283–S285.

[5] Ohira, Y., Yoshinaga, T., Ohara, M., Nonaka, I. *et al.*, Myonuclear domain and myosin phenotype in human soleus after bed rest with or without loading. *J. Appl. Physiol.* 1999, *87*, 1776–1785.

[6] Yamashita-Goto, K., Okuyama, R., Honda, M., Kawasaki, K. *et al.*, Maximal and submaximal forces of slow fibers in human soleus after bed rest. *J. Appl. Physiol.* 2001, *91*, 417–424.

[7] Trappe, S. W., Trappe, T. A., Lee, G. A., Widrick, J. J. *et al.*, Comparison of a space shuttle flight (STS-78) and bed rest on human muscle function. *J. Appl. Physiol.* 2001, *91*, 57–64.

[8] Trappe, S., Trappe, T., Gallagher, P., Harber, M. *et al.*, Human single muscle fibre function with 84 day bed-rest and resistance exercise. *J. Physiol.* 2004, *557*, 501–513.

[9] Berg, H. E., Dudley, G. A., Haggmark, T., Ohlsen, H., Tesch, P. A., Effects of lower limb unloading on skeletal muscle mass and function in humans. *J. Appl. Physiol.* 1991, *70*, 1882–1885.

[10] Larsson, L., Li, X., Berg, H. E., Frontera, W. R., Effects of removal of weight-bearing function on contractility and myosin isoform composition in single human skeletal muscle cells. *Pflugers Arch.* 1996, *432*, 320–328.

[11] Narici, M. V., Maganaris, C. N., Adaptability of elderly human muscles and tendons to increased loading. *J. Anat.* 2006, *208*, 433–443.

[12] Widrick, J. J., Knuth, S. T., Norenberg, K. M., Romatowski, J. G. *et al.*, Effect of a 17 day spaceflight on contractile properties of human soleus muscle fibres. *J. Physiol.* 1999, *516*, 915–930.

[13] D'Antona, G., Pellegrino, M. A., Adami, R., Rossi, R. *et al.*, The effect of ageing and immobilization on structure and function of human skeletal muscle fibres. *J. Physiol.* 2003, *552*, 499–511.

[14] Ferretti, G., Berg, H. E., Minetti, A. E., Moia, C. *et al.*, Maximal instantaneous muscular power after prolonged bed rest in humans. *J. Appl. Physiol.* 2001, *90*, 431–435.

[15] Widrick, J. J., Romatowski, J. G., Bain, J. L., Trappe, S. W. *et al.*, Effect of 17 days of bed rest on peak isometric force and unloaded shortening velocity of human soleus fibers. *Am. J. Physiol.* 1997, *273*, C1690–C1699.

[16] Gibson, J. N., Halliday, D., Morrison, W. L., Stoward, P. J. *et al.*, Decrease in human quadriceps muscle protein turnover consequent upon leg immobilization. *Clin. Sci.* 1987, *72*, 503–509.

[17] Ferrando, A. A., Lane, H. W., Stuart, C. A., Davis-Street, J., Wolfe, R. R., Prolonged bed rest decreases skeletal muscle and whole body protein synthesis. *Am. J. Physiol.* 1996, *270*, E627–E633.

[18] Ferrando, A. A., Paddon-Jones, D., Wolfe, R. R., Alterations in protein metabolism during space flight and inactivity. *Nutrition* 2002, *18*, 837–841.

[19] Biolo, G., Ciocchi, B., Lebenstedt, M., Barazzoni, R. *et al.*, Short-term bed rest impairs amino acid-induced protein anabolism in humans. *J. Physiol.* 2004, *558*, 381–388.

[20] Chen, Y. W., Gregory, C. M., Scarborough, M. T., Shi, R. *et al.*, Transcriptional pathways associated with skeletal muscle disuse atrophy in humans. *Physiol. Genomics* 2007, *31*, 510–520.

[21] Jones, S. W., Hill, R. J., Krasney, P. A., O'Conner, B. *et al.*, Disuse atrophy and exercise rehabilitation in humans profoundly affects the expression of genes associated with the regulation of skeletal muscle mass. *FASEB J.* 2004, *18*, 1025–1027.

[22] Ogawa, T., Furochi, H., Mameoka, M., Hirasaka, K. *et al.*, Ubiquitin ligase gene expression in healthy volunteers with 20-day bedrest. *Muscle Nerve* 2006, *34*, 463–469.

[23] Urso, M. L., Scrimgeour, A. G., Chen, Y. W., Thompson, P. D., Clarkson, P. M., Analysis of human skeletal muscle after 48 h immobilization reveals alterations in mRNA and protein for extracellular matrix components. *J. Appl. Physiol.* 2006, *101*, 1136–1148.

[24] Glass, D. J., Signalling pathways that mediate skeletal muscle hypertrophy and atrophy. *Nat. Cell. Biol.* 2003, *5*, 87–90.

[25] Sandri, M., Lin, J., Handschin, C., Yang, W. *et al.*, PGC-1alpha protects skeletal muscle from atrophy by suppressing FoxO3 action and atrophy-specific gene transcription. *Proc. Natl. Acad. Sci. USA* 2006, *103*, 16260–16265.

[26] Wu, Z., Puigserver, P., Andersson, U., Zhang, C. *et al.*, Mechanisms controlling mitochondrial biogenesis and respiration through the thermogenic coactivator PGC-1. *Cell* 1999, *98*, 115–124.

[27] Baar, K., Wende, A. R., Jones, T. E., Marison, M. *et al.*, Adaptations of skeletal muscle to exercise: rapid increase in the transcriptional coactivator PGC-1. *FASEB J.* 2002, *16*, 1879–1886.

[28] Lin, J., Wu, H., Tarr, P. T., Zhang, C. Y. *et al.*, Transcriptional co-activator PGC-1 alpha drives the formation of slow-twitch muscle fibres. *Nature* 2002, *418*, 797–801.

[29] Capitanio, D., Vasso, M., Fania, C., Moriggi, M. *et al.*, Comparative proteomic profile of rat sciatic nerve and gastrocnemius muscle tissues in ageing by 2-D DIGE. *Proteomics* 2009, *9*, 2004–2020.

[30] Moriggi, M., Cassano, P., Vasso, M., Capitanio, D. *et al.*, A DIGE approach for the assessment of rat soleus muscle changes during unloading: effect of acetyl-L-carnitine supplementation. *Proteomics* 2008, *8*, 3588–3604.

[31] Vigano, A., Ripamonti, M., De Palma, S., Capitanio, D. *et al.*, Proteins modulation in human skeletal muscle in the early phase of adaptation to hypobaric hypoxia. *Proteomics* 2008, *8*, 4668–4679.

[32] Doran, P., O'Connell, K., Gannon, J., Kavanagh, M., Ohlendieck, K., Opposite pathobiochemical fate of pyruvate kinase and adenylate kinase in aged rat skeletal muscle as revealed by proteomic DIGE analysis. *Proteomics* 2008, *8*, 364–377.

[33] O'Connell, K., Ohlendieck, K., Proteomic DIGE analysis of the mitochondria-enriched fraction from aged rat skeletal muscle. *Proteomics* 2009, *9*, 5509–5524.

[34] Chopard, A., Arrighi, N., Carnino, A., Marini, J. F., Changes in dysferlin, proteins from dystrophin glycoprotein complex, costameres, and cytoskeleton in human soleus and vastus lateralis muscles after a long-term bedrest with or without exercise. *FASEB J.* 2005, *19*, 1722–1724.

[35] Blottner, D., Salanova, M., Puttmann, B., Schiffl, G. *et al.*, Human skeletal muscle structure and function preserved by vibration muscle exercise following 55 days of bed rest. *Eur. J. Appl. Physiol.* 2006, *97*, 261–271.

[36] Bergstrom, J., Percutaneous needle biopsy of skeletal muscle in physiological and clinical research. *Scand. J. Clin. Lab. Invest.* 1975, *35*, 609–616.

[37] Rittweger, J., Frost, H. M., Schiessl, H., Ohshima, H. *et al.*, Muscle atrophy and bone loss after 90 days' bed rest and the effects of flywheel resistive exercise and pamidronate: results from the LTBR study. *Bone* 2005, *36*, 1019–1029.

[38] Taylor, C. F., Paton, N. W., Lilley, K. S., Binz, P. A. *et al.*, The minimum information about a proteomics experiment (MIAPE). *Nat. Biotechnol.* 2007, *25*, 887–893.

[39] Alban, A., David, S. O., Bjorkesten, L., Andersson, C. *et al.*, A novel experimental design for comparative two-dimensional gel analysis: two-dimensional difference gel electrophoresis incorporating a pooled internal standard. *Proteomics* 2003, *3*, 36–44.

[40] Tonge, R., Shaw, J., Middleton, B., Rowlinson, R. *et al.*, Validation and development of fluorescence two-dimensional differential gel electrophoresis proteomics technology. *Proteomics* 2001, *1*, 377–396.

[41] Karp, N. A., Kreil, D. P., Lilley, K. S., Determining a significant change in protein expression with DeCyder during a pair-wise comparison using two-dimensional difference gel electrophoresis. *Proteomics* 2004, *4*, 1421–1432.

[42] Karp, N. A., Lilley, K. S., Maximising sensitivity for detecting changes in protein expression: experimental design using minimal CyDyes. *Proteomics* 2005, *5*, 3105–3115.

[43] Marouga, R., David, S., Hawkins, E., The development of the DIGE system: 2D fluorescence difference gel analysis technology. *Anal. Bioanal. Chem.* 2005, *382*, 669–678.

[44] Viswanathan, S., Unlu, M., Minden, J. S., Two-dimensional difference gel electrophoresis. *Nat. Protoc.* 2006, *1*, 1351–1358.

[45] Benjamini, Y., Hochberg, Y., On the adaptive control of the false discovery rate in multiple testing with independent statistics. *J. Educ. Behav. Stat.* 2000, *25*, 60–83.

[46] Danieli Betto, D., Zerbato, E., Betto, R., Type 1, 2A, and 2B myosin heavy chain electrophoretic analysis of rat muscle fibers. *Biochem. Biophys. Res. Commun.* 1986, *138*, 981–987.

[47] Capelli, C., Antonutto, G., Kenfack, M. A., Cautero, M. *et al.*, Factors determining the time course of VO2(max) decay during bedrest: implications for VO2(max) limitation. *Eur. J. Appl. Physiol.* 2006, *98*, 152–160.

[48] Shang, X., Chen, S., Ren, H., Li, Y., Huang, H., Carbonic anhydrase III: the new hope for the elimination of exercise-induced muscle fatigue. *Med. Hypotheses* 2009, *72*, 427–429.

[49] Chopard, A., Lecunff, M., Danger, R., Lamirault, G. *et al.*, Large-scale mRNA analysis of female skeletal muscles during 60 days of bed rest with and without exercise or dietary protein supplementation as countermeasures. *Physiol. Genomics* 2009, *38*, 291–302.

[50] di Prampero, P. E., Narici, M. V., Muscles in microgravity: from fibres to human motion. *J. Biomech.* 2003, *36*, 403–412.

[51] Hoshijima, M., Mechanical stress-strain sensors embedded in cardiac cytoskeleton: Z disk, titin, and associated structures. *Am. J. Physiol. Heart Circ. Physiol.* 2006, *290*, H1313–H1325.

[52] Frey, N., Richardson, J. A., Olson, E. N., Calsarcins, a novel family of sarcomeric calcineurin-binding proteins. *Proc. Natl. Acad. Sci. USA* 2000, *97*, 14632–14637.

[53] Gong, H., Hatch, V., Ali, L., Lehman, W. *et al.*, Mini-thin filaments regulated by troponin-tropomyosin. *Proc. Natl. Acad. Sci. USA* 2005, *102*, 656–661.

[54] Udaka, J., Ohmori, S., Terui, T., Ohtsuki, I. *et al.*, Disuse-induced preferential loss of the giant protein titin depresses muscle performance via abnormal sarcomeric organization. *J. Gen. Physiol.* 2008, *131*, 33–41.

[55] Powers, S. K., Kavazis, A. N., McClung, J. M., Oxidative stress and disuse muscle atrophy. *J. Appl. Physiol.* 2007, *102*, 2389–2397.

[56] Li, W., Khor, T. O., Xu, C., Shen, G. *et al.*, Activation of Nrf2-antioxidant signaling attenuates NFkappaB-inflammatory response and elicits apoptosis. *Biochem. Pharmacol.* 2008, *76*, 1485–1489.

[57] Puscas, I., Coltau, M., Domuta, G., Baican, M. *et al.*, Carbonic anhydrase I inhibition by nitric oxide: implications for mediation of the hypercapnia-induced vasodilator response. *Clin. Exp. Pharmacol. Physiol.* 2000, *27*, 95–99.

[58] Westerheide, S. D., Anckar, J., Stevens, S. M.,Jr., Sistonen, L., Morimoto, R. I., Stress-inducible regulation of heat shock factor 1 by the deacetylase SIRT1. *Science* 2009, *323*, 1063–1066.

[59] Capitanio, D., Vigano, A., Ricci, E., Cerretelli, P. *et al.*, Comparison of protein expression in human deltoideus and vastus lateralis muscles using two-dimensional gel electrophoresis. *Proteomics* 2005, *5*, 2577–2586.

[60] Gelfi, C., De Palma, S., Cerretelli, P., Begum, S., Wait, R., Two-dimensional protein map of human vastus lateralis muscle. *Electrophoresis* 2003, *24*, 286–295.

[61] Hojlund, K., Yi, Z., Hwang, H., Bowen, B. *et al.*, Characterization of the human skeletal muscle proteome by one-dimensional gel electrophoresis and HPLC-ESI-MS/MS. *Mol. Cell. Proteomics* 2008, *7*, 257–267.

[62] Kovalyova, M. A., Kovalyov, L. I., Toropygin, I. Y., Shigeev, S. V. *et al.*, Proteomic analysis of human skeletal muscle (m. vastus lateralis) proteins: identification of 89 gene expression products. *Biochemistry* 2009, *74*, 1239–1252.

[63] Holloway, K. V., O'Gorman, M., Woods, P., Morton, J. P. *et al.*, Proteomic investigation of changes in human vastus lateralis muscle in response to interval-exercise training. *Proteomics* 2009, *9*, 5155–5174.

